Surveys in Geophysics (2024) 45:721–743
https://doi.org/10.1007/s10712-023-09820-w

High-Resolution Sonic Slowness Estimation Based on the Reconstruction of Neighboring Virtual Traces

Song Xu[1,2,3] · **Shun Li**[1] · **Zhihui Zou**[1,2,3]

Received: 12 September 2023 / Accepted: 1 December 2023 / Published online: 2 January 2024

Abstract
The estimation of elastic properties of thin-bed formations from sonic logging is challenging. Standard slowness processing of sonic logging waveforms typically yields an average slowness log profile over the span of the receiver array, obscuring thin-layer features smaller than the array aperture. In order to enhance vertical resolution of the slowness logs, the subarray processing techniques have been developed. However, for the subarrays with smaller aperture, the semblance from subarray waveforms becomes susceptible to noise, which results in a low signal-to-noise (S/N) ratio for the processing slowness logs. To overcome the above drawbacks, we propose a slowness estimation method with the enhanced resolution ranging from the conventional array aperture resolution to the inter-receiver spacing based on the reconstruction of neighboring virtual traces (RNVTs). The method utilizes super-virtual interferometry to reconstruct a large number of waveforms for slowness extraction using redundant information from overlapping receiver subarrays. We validate the feasibility and effectiveness of the proposed method using synthetic numerical experiments. By adding different levels of noise to synthetic data, we conclude that the new method has better noise robustness. Finally, we apply this method to field data, and the estimated high-resolution slowness logs show good agreement in interbedded sand-shale sequences. Both numerical tests and examples of field data show that, the slowness logs estimated by the new method can be obtained with a high resolution as well as with a high S/N ratio, providing an effective method for assessing slowness properties from a borehole.

Keywords Geophysical measurements · High resolution · Slowness estimation · Waveform reconstruction · Thin layer · Signal-to-noise ratio

Abbreviations

STC	Slowness-time coherence
ST	Slowness time
S/N	Signal-to-noise
SVI	Super-virtual interferometry
LWD	Logging while drilling
CAL	Caliper logging
SVI-SNV	Stacking of neighboring virtual-traces
RNVTs	Reconstruction of neighboring virtual traces

Extended author information available on the last page of the article

FTSE	Fast arrival time and slowness estimate
PML	Perfectly matched layer
GR	Gamma ray
VCL	Volume of shale

Article Highlights

- A slowness estimation method with the enhanced resolution is proposed based on the reconstruction of neighboring virtual traces (RNVTs)
- The improved results of synthetic data suggest the proposed method can extract thin layer slowness with both high-resolution and S/N ratio
- The application of the method has been tested and verified with field data

1 Introduction

Accurate extraction of valid information from measurement data is the key to understanding the composition of subsurface media. As one of the most effective means of estimating the velocity/slowness of rock formations, sonic logging has been used in a wide variety of applications, such as porosity calculations (e.g., Bassiouni 1994; Kazatchenko et al. 2003), seismic data processing and interpretation (e.g., Coates et al. 2000; Herrera and van der Baan 2014; Bader et al. 2017; Razak et al. 2021), petrophysical, elastic and formation mechanical evaluations, and lithological interpretation (e.g., Montmayeur and Graves 1985; Walls 1987; Paillet and Cheng 1991; Tang et al. 2004; Franco et al. 2006; Godio and Dall'Ara 2012; Assous et al. 2014). Therefore, the role of accurate extraction of sonic slowness is vital. In recent years, with the development of exploration/development of hydrocarbon reservoirs, higher requirements have been put forward for slowness extraction, especially for delicate thin layers. However, due to the limitation of the sonic tool resolution (aperture of the sonic receiver array), the logging response of the thin layer is insensitive, which results in the hiding or obscuring of the sonic characteristics (Tang and Patterson 2001; Peyret et al. 2006). Additionally, low data quality (Wang et al. 2021b), formation anisotropy (Zeroug et al. 2018; Xu 2023b), noise disturbance (Xu et al. 2022; Xu 2023a), and spatial averaging effect (Oyler et al. 2008; Huang and Torres-Verdín 2016; Maalouf and Torres-Verdín 2018b) complicate the sonic data processing (Razak et al. 2021; Xu et al. 2022; Xu 2023a). The above effects cause the imprecise results of the slowness estimation, bringing great difficulties for the thin interlayer feature inscription.

In sonic logging, array processing methods have been used to estimate the sonic slowness with non-identical vibrational phases. Examples of them include slowness time coherence (STC) method (e.g., Neidell and Taner 1971; Kimball and Marzetta 1984; Hsu and Chang 1987; Bose et al. 2009), Nth-root method (McFadden et al. 1986), Prony algorithm (Lang et al. 1987; Tang 1997; Ma et al. 2010; Sun et al. 2019a), maximum-likelihood method (Hsu and Baggeroer 1986), matrix pencil algorithm (Ekstrom 1995; Wang et al. 2012; Chen et al. 2020), weighted spectral semblance and phase estimation algorithm (Nolte et al. 1997; Tang 1997; Kozak et al. 2006; Kozak and Williams 2015; Li et al. 2015), differential phase method (Mukhopadhyay et al. 2013; Zeng et al. 2018; Wang et al. 2021a), inversion-based method with a spatial sensitivity function or deconvolution (Huang and Torres-Verdín 2015, 2016, 2017; Maalouf and Torres-Verdín 2018b, a; Lei et al. 2019),

and fast arrival time and slowness estimate (FTSE) (Khadhraoui et al. 2018). It is worth noting that thin layers pose significant challenges to reservoir identification and evaluation. Conventional logging methods are inadequate for thin layers, making it difficult to accurately assess their characteristics, including oil-bearing properties, physical attributes, and electrical characteristics. In the context of acoustic well logging, conventional processing typically yields an average slowness profile over the span of the receiving array, which can mask true information of the thin layer if the thin layer thickness is less than the length of the subarray. This limitation hampers various aspects such as exploring oil in thin layers, storage energy evaluation, and formulation of development plans. The impact of thin layers is evident in three main aspects. Firstly, the thinness of the reservoir complicates the identification of lithology due to the interaction of various fine sandstones. Secondly, accurately identifying oil layers and determining effective thickness is challenging, leading to frequent misinterpretations. Thirdly, conventional logging struggles to reflect the true logging response of thin layers, resulting in inaccuracies in parameters such as water saturation, oil and gas content, porosity, saturation, permeability, and clay content. This, in turn, affects the objective assessment of reserves. To obtain higher resolution sonic velocities, one of the commonly used methods is multi-shot subarray technique (Hsu and Chang 1987). This method utilizes well sonic data at the same depth with subarray apertures to obtain various resolution slowness logs and has been extended in both the time (Tang et al. 1995; Valero et al. 2000; Zhang and Tang 2000; Tang and Patterson 2001; Mahiout et al. 2022) and frequency domains (Brie et al. 1988; Wang et al. 2018; Sun et al. 2019b). Subarray processing using small apertures would enrich the waveform data combinations. However, in some specific combinations, the signal-to-noise (S/N) ratio of the subarray processing logs is low due to insufficient data volume. For instance, a combination of 15.24 cm aperture subarrays (i.e., only 2 receivers spanning 15.24 cm) is the highest resolution configuration, while its processing results have a low S/N ratio because of participant data usage limits (Tang et al. 2004). Other methods, mainly based on inversion, have recently been proposed to obtain thin-layer elastic properties. Huang and Torres-Verdín (2015), Huang and Torres-Verdín (2016), Huang and Torres-Verdín (2017), Maalouf and Torres-Verdín (2018b), and Maalouf and Torres-Verdín (2018a) proposed an inversion method of spatial sensitivity function. This method is constructed from a geometric model consisting of uniformly horizontal rock layers penetrated by boreholes orthogonal to the rock layers. The boundaries of the thin layers should be accurately defined in advance to avoid excessive smoothing of the inversion solution. Lei et al. (2019) proposed a multi-scale resolution inversion method based on linear convolutional model, but this method will not be able to resolve the stratification below the inch scale. In addition, the combined model-driven and data-driven slowness estimation method proposed by Khadhraoui et al. (2018) can provide stable wave arrivals and improve the accuracy of compressional waves slowness estimation.

Super-virtual interferometry (SVI) (Bharadwaj et al. 2011; Hanafy et al. 2011; Mallinson et al. 2011; Bharadwaj et al. 2012; Lu et al. 2020) provides a mean for solving the difficulties above. Super-virtual interferometry is originally derived from seismic interferometry (Claerbout 1968; Wapenaar et al. 2005; Wapenaar and Fokkema 2006; Wapenaar et al. 2010a, b; Dong et al. 2006; Schuster 2009), this method was first used to enhance head waves of seismic refraction (Bharadwaj et al. 2011, 2012; Mallinson et al. 2011; Hanafy et al. 2011; Hanafy and Al-Hagan 2012; Alshuhail et al. 2012; Bharadwaj et al. 2013; Al-Hagan et al. 2014; Qiao et al. 2014, 2015; An et al. 2017). Xu et al. (2017) applied SVI to sonic logging for casing wave suppression, effectively improving the S/N ratio of the target array waveform and opened a door for array processing. Subsequently, the method has been successfully applied to suppress drill

Fig. 1 Schematic diagram of the proposed method. **a** depicts various subarray combinations for an 8-receiver array, totaling seven possible subarray configurations for the array-acoustic tool, each with distinct resolutions. **b** Combination of subarrays with 60.96-cm aperture. Four sets of data from identical depth layers (blue circles) are available for utilization, representing the same geological information at the same resolution. The construction of neighboring is exemplified virtual traces under various resolution combinations using the cross-correlation of events within the pink box in (**c**). In reconstructing the target waveform within the pink box in (**d**), virtual traces from cross-correlation of adjacent events within the resolution span are employed, as indicated by the red box in (**d**). In the 60.69-cm resolution range, neighboring event cross-correlation is partitioned into four combinations, each comprising 7 correlations, illustrated in (**e**). It is noteworthy that waveform construction within the combination span utilizes neighboring virtual traces from all logging data within the same depth interval. Solid pentagrams represent sound sources, while hollow pentagrams underscore real sources not used in interference processing, emphasizing that cross-correlation originates from virtual sources (green pentagrams) excited and recorded by the receiver

collar waves and other disturbing noise (Dawood et al. 2021; Xu and Zou 2023). It is worth mentioning that Xu and Zou (2023) extended the application of SVI to acoustic scenarios in logging while drilling (LWD), effectively enhancing signal-to-noise ratios in routine data processing. However, it is noteworthy that their work lacks a detailed exposition on high-resolution velocity/slowness analysis. Additionally, the underutilization of information from newly neighboring virtual traces has resulted in the insufficient exploitation of valuable formation signals, highlighting a critical area for improvement and enhancement in this current research. Furthermore, SVI has great potential as an effective noise suppression and S/N ratio improvement method for logging applications. SVI constructs retrieved waveforms using far-field reciprocal equation (Wapenaar and Fokkema 2006; Schuster 2009), and this Green's function-based retrieval is driven by pure data. As a result, the S/N ratio of the reconstructed data can be increased with the number of sources and receivers used. In sonic logging, the array aperture moves only a small fraction of its length between consecutive source shots, allowing for a wealth of redundant information to be obtained in consecutive shots and acquisitions due to the diversity of overlapping depth intervals. This means that SVI is highly scalable for methods using multiple sources and receivers such as multi-shot processing. The super virtual interferometry method, based on the stacking of neighboring virtual-traces (SVI-SNV), proposed by Song et al. (2019) brings more possibilities to multi-shot processing techniques. SVI-SNV exploits the delayed nature of cross-correlation to generate more virtual traces to be superimposed, improving the accuracy of the virtual channels involved in reconstruction to enhance the S/N ratio.

In this paper, we propose an enhanced-resolution slowness estimation method based on the reconstruction of neighboring virtual traces (RNVTs). We firstly derive the formulae and describe the RNVTs involved in extracting sonic waveforms. The proposed method details the combination of waveform data at different slowness extraction resolutions for conventional 6, 8, and 12 receiver arrays. In the following, we use the pseudo-spectral approach to simulate sonic logging of a depth section containing thin layers. The noise immunity of the process is then tested at different resolutions, and the effect of resolution on slowness extraction is analyzed in detail. Finally, this method is applied to in field sonic logging data, and the slowness results with enhanced resolution are compared with lithological variation. The numerical tests and field data applications demonstrate that this method can extract slowness with both high-resolution and high S/N ratio, thus offering a useful tool for slowness estimation.

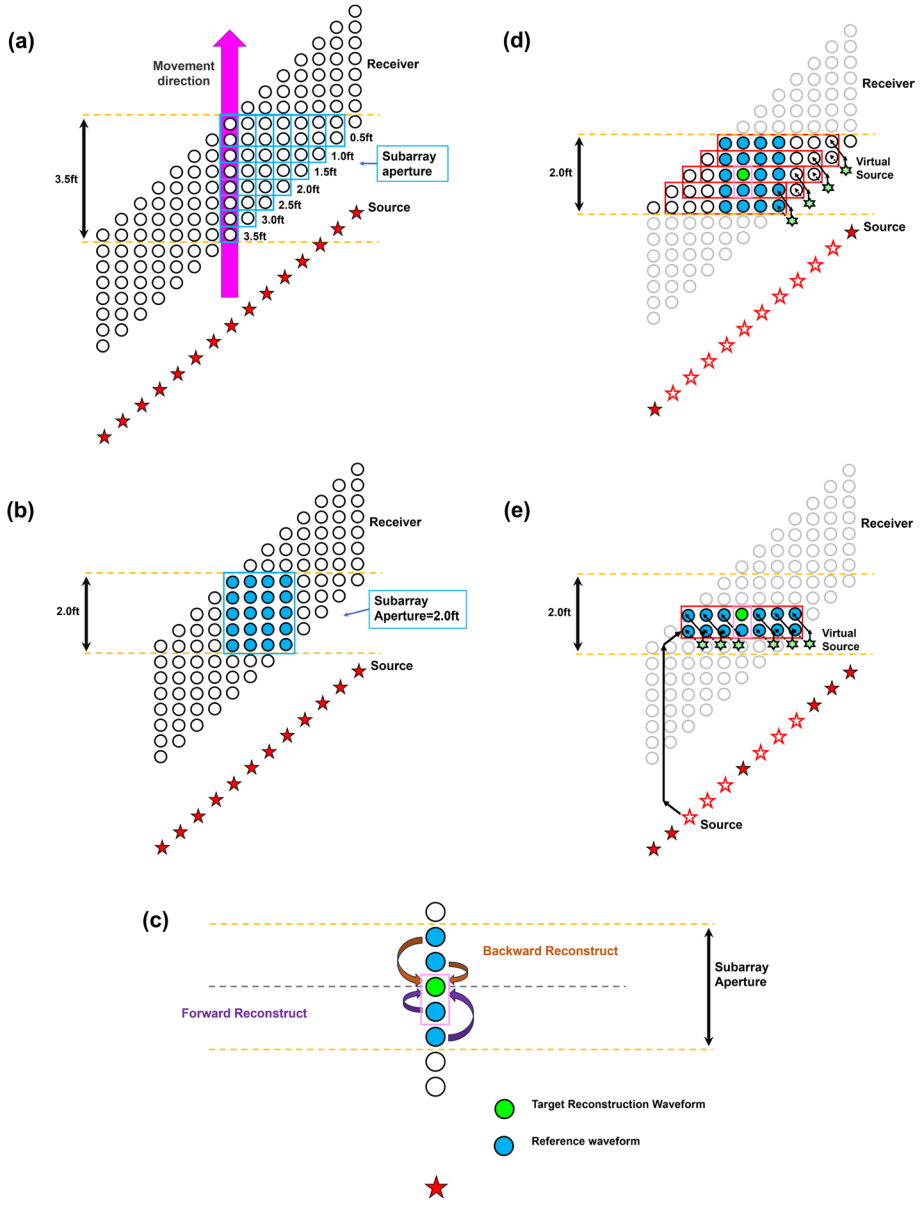

2 Methodology

The STC (e.g., Neidell and Taner 1971; Kimball and Marzetta 1984) is a commonly used method for obtaining the formation slowness from array sonic waveforms recorded by array sonic tools, which is also a basis for the methodology of this paper. This method scans the waveform data for wave arrival time and array data slowness (time in one dimension and slowness in the second dimension) based on the coherence of the

array data, and searches for the arrival time and slowness corresponding to the target waves in the array waveform at the extremes of the semblance function. Figure 1a displays the combinations of data at different resolutions using an array of 8 receivers as an example. Multiple subarrays from different source shots can be used for the same depth band. Therefore, the coherence functions of the different subarrays need to be calculated separately. For a subarray, the coherence can be defined using semblance method as

$$\mathrm{r}_M(\mathrm{Slow}, T) = \frac{X_{\mathrm{Co}}(\mathrm{Slow}, T)}{M \cdot X_{\mathrm{Inco}}(\mathrm{Slow}, T)} \tag{1}$$

where r_M is the semblance of a subarray of M receivers; X_{Co} is the stacked energy of the subarray data; X_{Inco} is the total energy of the subarray data; *slow* and T represent the slowness and arrival time. The stacked energy and the total energy can be defined as

$$X_{\mathrm{Co}}(\mathrm{Slow}, T) = \int_{T}^{T+T0} \left| \sum_{k=\psi}^{L} C_k(t + t_k) \right|^2 \mathrm{d}t \Big|_{\psi=1,2,\ldots,N-M+1}^{L=M+\psi-1} \tag{2}$$

and

$$X_{\mathrm{Inco}}(\mathrm{Slow}, T) = \int_{T}^{T+T0} \sum_{k=\psi}^{L} \left| C_k(t + t_k) \right|^2 \mathrm{d}t \Big|_{\psi=1,2,\ldots,N-M+1}^{L=M+\psi-1} \tag{3}$$

where C_k is the kth receiver of an array, $T0$ is processing time window; N represents the total number of the array receiver, M represents the number of the subarray receiver; ψ represents the index of the subarray at the same depth. t_k is the time the waveform moves to the kth receiver on the time axis, which can be expressed as follows

$$t_k = \mathrm{Slow}(k-1)d \tag{4}$$

where d is the minimum distance between two adjacent receivers in a receiver array. The semblance of a subarray can be obtained according to Eqs. (1)–(4).

At each depth interval spanned by a subarray, multiple subarray data sets overlap. Finally, the semblance of all subarrays in the same depth interval are superimposed and averaged. However, the arrays have different transmit-to-receive intervals, which means that a wave component has a different arrival time for each subarray (Valero et al. 2000). Such differences in the time of arrival make it difficult to combine the data. For the slowness time (ST) plane, direct superposition of subarray ST planes in the time and slowness domains can be achieved by time shifting (Valero et al. 2000). Another approach is to project the two-dimensional coherence function of each subarray onto the slowness axis, making it a one-dimensional function whose variable is slowness (Tang et al. 2004). This one-dimensional coherence function is expressed as follows:

$$\mathrm{r}_m(\mathrm{Slow}) = r_m(\mathrm{Slow}, T_{\mathrm{Max}})\Big|_{m=1\ldots N-M+1} \tag{5}$$

where T_{Max} is the arrival time at which the coherence function is extremely large; m represents the the mth subarray or mth semblance combination. The one-dimensional coherence functions of all subarrays can be stacked using either the algebraic mean or the geometric mean (Kimball and Marzetta 1984; Valero et al. 2000; Tang et al. 2004).

$$\overline{\mathrm{r}_m}(\mathrm{Slow}) = \frac{1}{N-M+1}\sum_{m=1}^{N-M+1}\mathrm{r}_m(\mathrm{Slow}) \tag{6}$$

or

$$\overline{\mathrm{r}_m}(\mathrm{Slow}) = \left[\prod_{m=1}^{N-M+1}\mathrm{r}_m(\mathrm{Slow})\right]^{\frac{1}{N-M+1}} \tag{7}$$

It should be noted that in subsequent studies presented in this paper, the analysis is conducted using Eq. 6.

We introduce super-virtual interferometry into multisource processing. Using super-virtual interferometry, more reconstructed waveforms can be used to extract slowness. Super-virtual interferometry based on neighboring virtual channels cleverly exploits the nature of cross-correlations (Dong et al. 2006; Song et al. 2019; Liang et al. 2020), which can be well suited to highly regular observing systems such as logging or multiple coverage (Xu and Zou 2023). For events received by two receivers excited by the same source, if the channel spacing of the two receivers is kept equal, the virtual traces generated by their cross-correlation will have the same delay time, i.e., the peaks of the virtual waveforms generated by different events are located at in same position. Therefore, in the waveform reconstruction process, the same reference channel can be used to convolve with these neighboring virtual channels, thus enabling multiple reconstructions of the target waveform. Figure 1b–e shows the waveform reconstruction in detail based on neighboring virtual channels, using the example of processing at a resolution of 60.96 cm. Figure 1b illustrates the combination of data at 60.96 cm resolution. The blue box shows the waveform data to be used for the slowness extraction, which consists of four subarrays. For a better understanding of reconstruction based on neighboring traces, Fig. 1c shows the reconstruction scheme of a specific waveform, and the target waveform reconstruction can be achieved by forward and backward processing (Xu and Zou 2023). For events recorded at neighboring receivers excited by the same source (the event in pink box in Fig. 1c, i.e., processing interval is one receiver spacing length), the target waveform can be reconstructed by convolving the reference channel with the virtual channels, where the virtual channels are generated by cross-correlation of all adjacent received events in the processed depth interval, as shown in Figs. 1d and e. In this case, a total of 27 target waveforms can be reconstructed with a processing interval of 1 receiver spacing. It should be noted that the virtual channels generated for cross-correlation between the target reconstruction channels and the reference channels are not included in the convolution calculation. (The event in the pink box Fig. 1e.)

Stacking of neighboring virtual-traces (SVI-SNV) mainly uses reciprocity equations of correlation and convolution types for the reconstruction of waveforms. For subarrays with dip receivers, the virtual waveforms based on SNV in same depth interval can be expressed as

$$\begin{aligned}&\mathrm{Im}\left[P^{F}_{vir}\left(L_j|L_{j+\lambda}\right)\right]\\ &= k\sum_{d=\vartheta+\theta+\omega}^{\vartheta+\theta+\sigma+\omega}\sum_{j=1}^{N-\lambda}P\left(L_{j+\lambda}|S_d\right)^{*}P\left(L_j|S_d\right)\Bigg|_{\substack{\lambda=1,2,\ldots,dip-1\\ \theta=\lambda-dip+1\\ \sigma=N-\lambda-1\\ \omega=0,\ldots,dip-\lambda-1}}\end{aligned} \tag{8}$$

and

$$\begin{aligned}&\mathrm{Im}\left[P_{vir}^{B}\left(L_{j+\lambda}|L_{j}\right)\right]\\&=\quad k\sum_{d=\vartheta+\theta+\omega}^{\vartheta+\theta+\sigma+\omega}\sum_{j=1}^{N-\lambda}P\left(L_{j}|S_{d}\right)^{*}P\left(L_{j+\lambda}|S_{d}\right)\Bigg|_{\substack{\lambda=1,2,\ldots,dip-1\\ \theta=\lambda-dip+1\\ \sigma=N-\lambda-1\\ \omega=0,\ldots,dip-\lambda-1}}\end{aligned}\tag{9}$$

where ϑ represents the depth corresponding to the data to be processed; P_{vir}^{F} represents the virtual waveform obtained by forward processing, P_{vir}^{B} represents the virtual waveform obtained by reverse processing, and $P(L_j|S_d)$ represents an event excited by a source with depth at d and received by the jth receiver of the receiving array L. N is the maximum number of receivers in the receiver array, dip is the maximum number of receivers contained in the subarray, Im is the imaginary part of the complex domain, k is the wavenumber, and * is the complex conjugate.

The reconstructed waveforms can be obtained by convolving the reference waveform with virtual waveform events having the same delay time. The waveform reconstruction for forward and backward processing can be expressed as follows

$$\begin{aligned}P_{\mathrm{Rec}}^{F}(L_{\delta F}^{c}|S_{c})=&2ik\sum_{\lambda=1}^{dip-1}P_{vir}^{F}(L^{d}|L_{\lambda}^{d})\\&\times\left(\sum_{RF=1}^{dip-\lambda}P(L_{RF}^{c}|S_{c})\right)\Bigg|_{\substack{c=\vartheta,\vartheta+1,\ldots,\vartheta+N-dip\\ \delta F=RF+\lambda}}\end{aligned}\tag{10}$$

and

$$\begin{aligned}P_{\mathrm{Rec}}^{B}(L_{\delta B}^{c}|S_{c})=&2ik\sum_{\lambda=1}^{dip-1}P_{vir}^{B}(L_{\lambda}^{d}|L^{d})\\&\times\left(\sum_{BF=1}^{dip-1}P(L_{BF+\lambda}^{c}|S_{c})\right)\Bigg|_{\substack{c=\vartheta,\vartheta+1,\ldots,\vartheta+N-dip\\ \delta B=BF}}\end{aligned}\tag{11}$$

where $P_{\mathrm{Rec}}^{F}(L_{\delta F}^{c}|S_{c})$ is the reconstructed forward processing waveform excited by a source S_c and received by receiver $L_{\delta F}^{c}$, $P_{\mathrm{Rec}}^{B}(L_{\delta B}^{c}|S_{c})$ is the reconstructed backward processing waveform excited by a source S_c and received by receiver $L_{\delta B}^{c}$, i represents an imaginary unit $i=\sqrt{-1}$. Ultimately, for a subarray, the reconstructed waveform can be expressed as

$$P_{\mathrm{Rec}=}P_{\mathrm{Rec}}^{F}+P_{\mathrm{Rec}}^{B}\tag{12}$$

where P_{Rec} is the reconstructed waveform, P_{Rec}^{F} is the forward processed reconstructed waveform, and P_{Rec}^{B} is the backward processed reconstructed waveform. The reconstructed waveforms were superimposed on the original waveforms and slowness was estimated using Eqs. (1)–(7).

Ultimately, we have listed the number of waveforms used at different resolutions for the 8-receiver array based on combinations of data, as shown in Table 1. In the table, *OW* is the number of original waveforms, *Dip* is the number of receivers in the subarray, *N* is

Table 1 The number of waveforms used in array of 8 receivers

Receiver_Number=8							
OW	Dip	N	Reconstructed waveforms				Total
			FRW	BRW	F+B	(F+B)*N	
14	2	7	6	6	12	84	98
18	3	6	31	31	62	372	390
20	4	5	86	86	172	860	880
20	5	4	180	180	360	1440	1460
18	6	3	320	320	640	1920	1938
14	7	2	511	511	1022	2044	2058
8	8	1	756	756	1512	1512	1520

the maximum number of subarrays available in the data combination, *FRW* is the number of forward reconstructed waveforms (abbreviated as *F*), *BRW* is the number of backward reconstructed waveforms (abbreviated as *B*), and *Total* is the sum of the number of original waveforms and the number of reconstructed waveforms. All reconstructed waveforms are superimposed on the original waveforms to achieve high-resolution and high S/N ratio extraction of slowness. For other common array processing, such as 6-receiver arrays and 12-receiver arrays, we also detail the number of waveforms available for different combinations of resolutions for the proposed method (Tables 2 and 3).

3 Numerical Simulation

To analyze and test the slowness extraction results of the proposed method, a thin interbeds simulation model is designed as shown in Fig. 2. To simulate the borehole logging acquisition, the blue area is fluid water with a diameter of 0.10 m. Eight thin layers of 0.45 m thickness are inserted into the background formation at equal intervals. The thin-layer velocities are designed to increase layer by layer to better demonstrate the effect of subarray processing on resolution. The detailed physical parameters can be seen in Table 4. The simulation is performed using the pseudo-spectral method (Kosloff and Baysal 1982; Kosloff et al. 1984), with the monopole source using a standard Ricker wavelet with a center frequency of 10 kHz. The 0.005-m square grids with an iterative time step of 0.5 microseconds are used in the synthetic model. A perfectly matched

Table 2 The number of waveforms used in array of 6 receivers

Receiver_Number=6							
OW	Dip	N	Reconstructed waveforms				Total
			FRW	BRW	F+B	(F+B)*N	
10	2	5	4	4	8	40	50
12	3	4	21	21	42	168	180
12	4	3	58	58	116	348	360
10	5	2	120	120	240	480	490
6	6	1	210	210	420	420	426

Table 3 The number of waveforms used in array of 12 receivers

Receiver_Number=12							
OW	Dip	N	Reconstructed waveforms				Total
			FRW	BRW	F+B	(F+B)*N	
22	2	11	10	10	20	220	242
30	3	10	51	51	102	1020	1050
36	4	9	142	142	284	2556	2592
40	5	8	300	300	600	4800	4840
42	6	7	540	540	1080	7560	7602
56	7	6	875	875	1750	10,500	10,556
40	8	5	1316	1316	2632	13,160	13,200
36	9	4	1568	1568	3136	12,544	12,580
30	10	3	2550	2550	5100	15,300	15,330
22	11	2	3355	3355	6710	13,420	13,442
12	12	1	4290	4290	8580	8580	8592

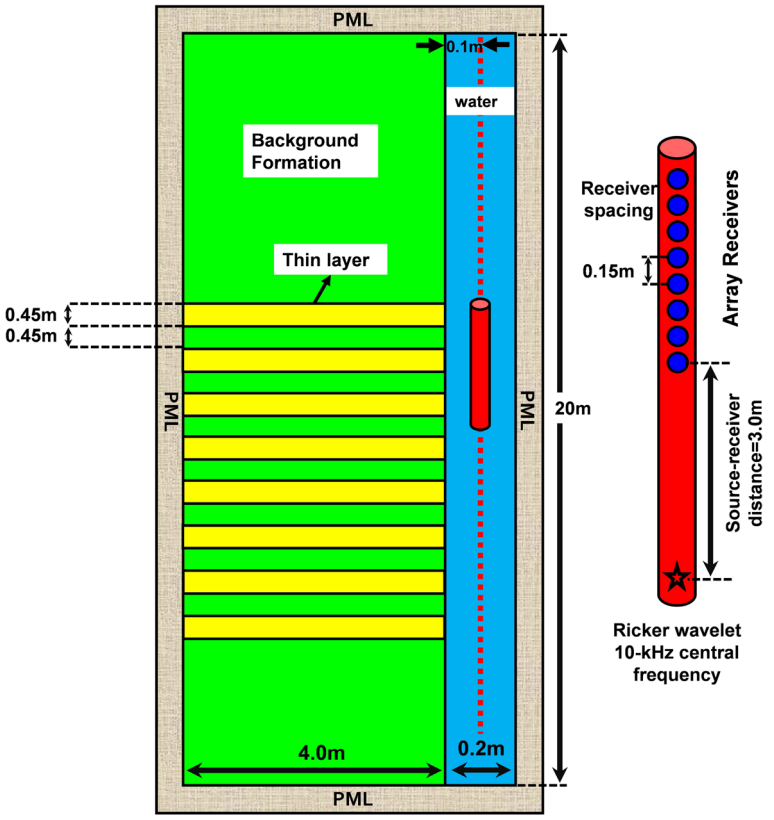

Fig. 2 The 2D thin interlayer simulation model. The model is 20-m long and 4.2-m wide. The green area is the background formation, the yellow area are the thin beds with the thickness of 0.45 m, and the blue area is the liquid water. The detailed physical parameters can be found in Table 4. The source of the monopole is the Ricker wavelet with a center frequency of 10 kHz. The sonic tool is moving along the red dotted line at 0.15 m intervals, with a source distance of 3.00 to 4.05 m

Table 4 Simulation Model Parameters

Material components	P-wave velocity (m/s)	S-wave velocity (m/s)	Density (kg/m^3)
Water fluid	1500		1000
Background formation	4000	2000	2300
Thick beds	2100+50*n	1050+25*n	2000

n represents the nth thin layer from shallow to deep ($n = 1, 2, \ldots, 8$)

layer (PML) with a thickness of 20 meshes is used to avoid boundary reflections (Ma et al. 2018; Xu et al. 2023). In the simulation, the sonic tool was moved to depth in 0.15-m increments, with the first receiver of the sonic array located 3.00 m from the monopole source. Figure 3 displays the simulated results.

The simulated waveforms of receiver 1 and receiver 8 of an eight-receiver array are shown in panels 1 and 2 of Fig. 3. The P-wave arrivals are clearly visible, and the waveforms in panel 2 appear in the background with a much weaker amplitude due to the source-receiver distance. For the thin layers of 0.45 m thickness (exactly the length of 3 receiver spacings), we first compare conventional STC processing to subarray processing with 45.72 cm resolution. Obviously, single-shot subarray processing shown in panel 4 yields more accurate thin-layer slowness compared with panel 3. The processing span of conventional STC is larger than the thickness of the thin layer, masking the effective information of the horizontal thin layer. However, compared to the conventional STC method, single-shot subarray processing uses less data, resulting in weaker convergence of the semblance correlogram.

In order to further analyze the actual acquisition scenarios, we performed noise immunity tests for both processes. The noise is imposed in three levels, 30%, 50%, and 70% of the maximum value of the P wave amplitude. Panel 1 of Fig. 4 shows the waveform data with random noise added and the semblance results are displayed in Panels 2 and 3 of Fig. 4. At low noise levels, conventional STC process and subarray process can extract some of the slowness information. However, as the noise level increases, the P-wave arrivals become more difficult to identify. As a result, this makes accurate slowness extraction difficult to achieve. Meanwhile, the distinguished results reveal the main weaknesses of high-resolution processing. Since less waveform data are used, the subarray processing is less capable of resisting noise.

The method proposed in this paper is able to overcome the above-mentioned shortcomings. The depth increment is typically equal to the inter-receiver spacing of the receiver array when using array sonic tools. Therefore, the subarrays at successive source positions can be overlapping. An important feature of SVI is that the noise reduction effect is positively correlated with the number of sources and receivers used. The newly proposed method combines multi-shot processing and SVI-SNV to obtain high S/N ratio slowness profiles using a large amount of reconstructed data. This is confirmed by the results of the comparison between the single-shot processing and the proposed method in Fig. 5 (both using the vertical resolution of 45.72 cm). P-wave coherence converges well at all three levels of noise addition, as shown in the right side of Panels 1, 2, and 3 of Fig. 5. Another point to be clarified is that the range of convergence of P-wave coherence varies with the difference in noise levels. This can affect the accurate extraction of thin bed information. In addition, there are artifacts in the

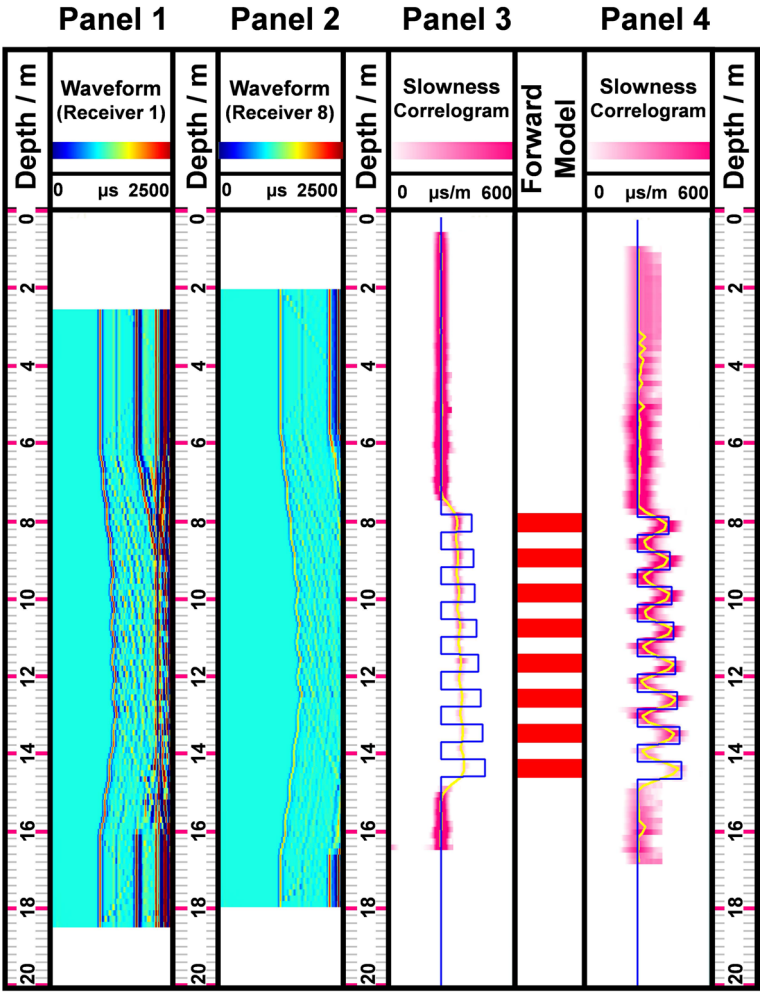

Fig. 3 Schematic of noise-free synthetic data. Panels 1 and 2 show full simulation waveform at receiver 1 and receiver 8 of an array of eight receivers, respectively. The P-wave is clearly visible, and the waveform amplitudes at receiver 8 are weaker due to the source distance. Panels 3 and 4 show the semblance correlogram of the array waveforms using the conventional semblance method (array aperture = 106.68 cm) and subarray processing method (subarray aperture = 45.72 cm), respectively. The results show that the subarray aperture cannot reflect the true slowness information of the thin bed if it is larger than the thickness of the thin bed

waveform reconstructed by the SVI. However, the effect produced by these artifacts is negligible. The slowness obtained from the artifacts is the same as the real waveform and therefore the results of the slowness projection in the depth domain are unaffected.

For the final step of the numerical experiments, we tested the accuracy of the extracted slowness at different resolutions, as shown in Fig. 6. The vertical resolution of sonic logging is largely controlled by the tool aperture, and thin layer smaller than the array aperture tend to be more difficult to detect or identify. The experiment in Fig. 6 shows the effect of this difference in detail. Panels 5–8 show the results of processing with a resolution greater than

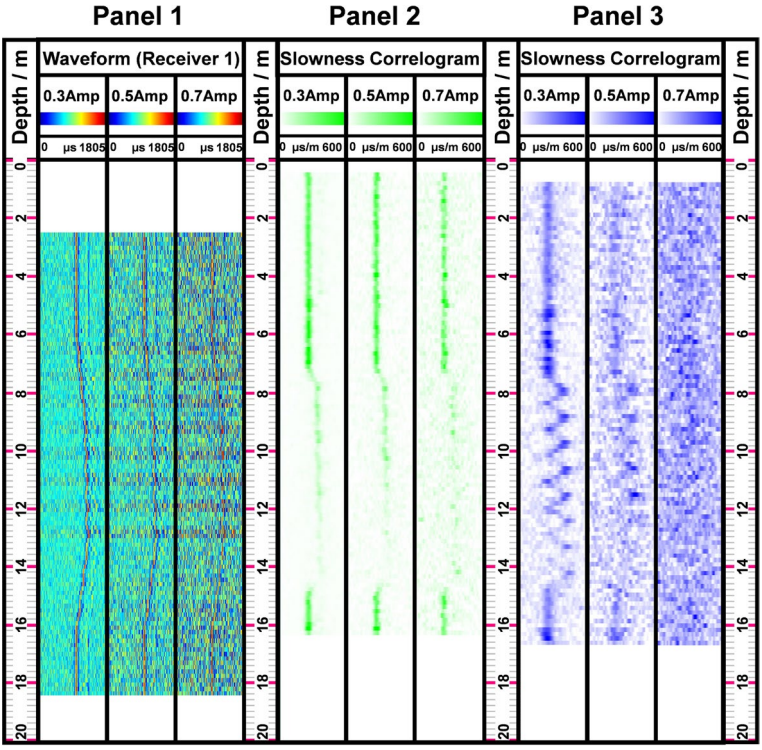

Fig. 4 Noise immunity test results for subarray apertures of 106.68 cm versus 45.72 cm. Random noise was used in the test. The semblance correlogram of the array waveforms of the conventional and sub-array treatments under noise addition are shown in panels 2 and 3. As the noise increases, both methods of single shot processing produce worse results. The results show that treatments with a subarray aperture of 45.72 cm are able to extract a certain amount of slowness at a noise level of 0.3 maximum amplitude. However, as the noise increases, it is unable to obtain slowness from the waveform recordings

the thin layer thickness. Increasing the array aperture results in the sonic log providing a spatially averaged slowness, and the true thin layer characteristics are masked. Panels 2–4 show the results obtained when the subarray aperture is equal or smaller than the thin layer. The changes in P-wave slowness are clearly visible on the semblance correlogram. Another noteworthy phenomenon is that the degree of convergence of P-wave coherence obtained from subarray processing at different resolutions is inconsistent. This is due to the number of reconstructed waveforms used depending on the data combination. For example, for an sonic tool with 8 receivers, the number of waveforms available for processing at the highest resolution is small. (Details are provided in Table 1.) This also explains that the processing results with the highest resolution shown in panel 2 of Fig. 6 are not relatively robust. Therefore, it is suggested that a combination of subarrays with more available waveforms should be chosen for elastic properties extraction of thin beds.

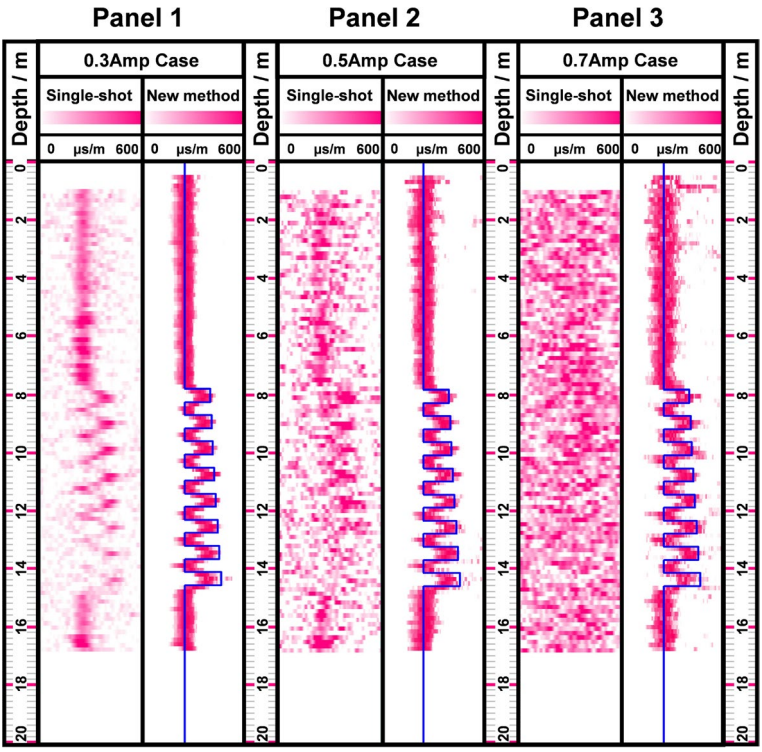

Fig. 5 Comparison of the results of the new method proposed with the single-shot subarray processing method at 45.72 cm vertical resolution (i.e., the Subarray Aperture). The RNVTs yields semblance results with both high vertical resolution and high S/N ratio, indicating the validity of the method

4 Application

In this section, field data are used to verify the performance and reliability of the technique. The results are shown in Fig. 7. Panel 1 shows the caliper and gamma-ray (GR) log curves for a 35 m formation interval containing sandstone with thin beds of shale. Panel 2 shows the full waveform recording in a time window from 0 to 1500 microseconds. The P-wave slowness is extracted using the proposed method with a resolution of 106.68 cm, a resolution of 45.72 cm, and a resolution of 15.24 cm. The related semblance correlogram are shown in panels 3, 4, and 5 of Fig. 7, respectively. The results of the semblance for the 3 resolutions mentioned above are consistent in their general trend. However, compared to the full array aperture results, the 45.72-cm and 15.24-cm resolution treatments have a higher sensitivity to formation response. Furthermore, the coherence of the waveforms will show different convergence depending on the amount of data used, as analyzed above. The slowness curves for each of the three resolutions are shown in panels 6–8. Based on the gamma ray and porosity logs, thin shales are likely to be present at depths of X702–704 m, X717–718 m, X722–724 m, X726–727 m, and X731–732 m. This is basically consistent with the fluctuations in slowness curves of panels 7 and 8, further confirming the validity and reliability of the proposed method. The conventional resolution slowness curves do not reflect the corresponding thin beds information due to the large processing aperture.

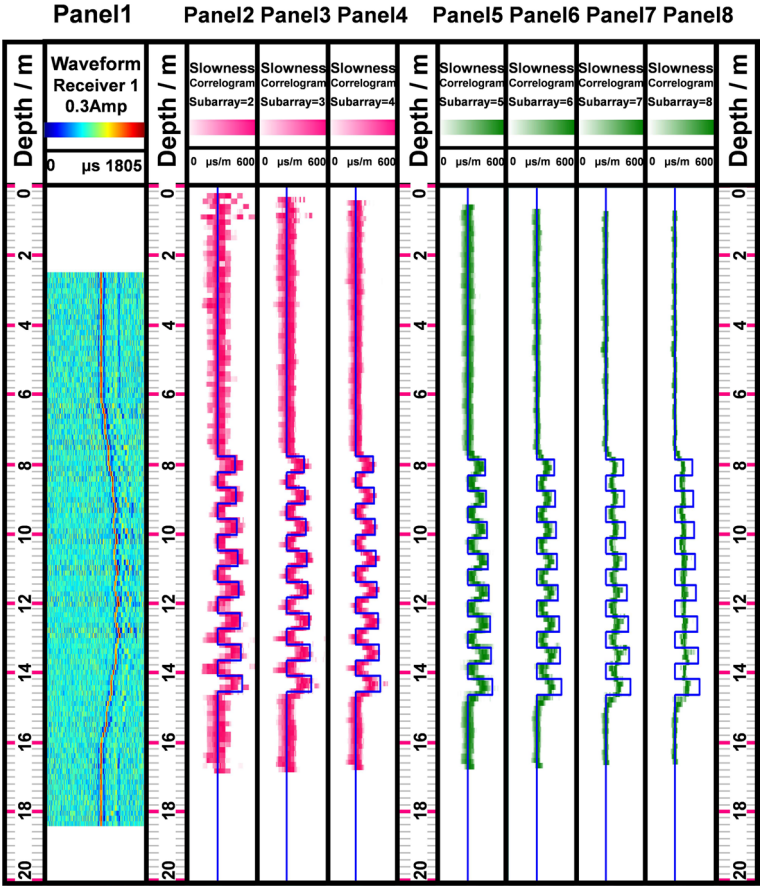

Fig. 6 Semblance results for different subarray apertures at 0.3 maximum amplitude level of added noise. The additive noise waveforms of array receiver 1 are shown in panel 1. Panels 2 to 4 show the results of processing with a subarray size smaller than the thickness of the thin bed, whose semblance correlograms are colored in pink. Panels 5 to 8 demonstrate the results of processing with a resolution greater than the thickness of the thin bed, whose semblance correlograms are colored in green. The results show that the exact properties (slowness) can be accurately estimated if the processing subarray size is less than the thickness of the thin bed

To further demonstrate the effectiveness of slowness processing results at different resolutions, we conducted a quantitative assessment of the data, and the results are shown in Fig. 8. The results in Fig. 8a illustrate the correlation between three slowness resolutions, GR, and volume of shale (VCL). The lower correlation between the three slowness resolutions indicates differences among the processing results, precisely caused by the variations in resolution. Additionally, an interesting observation is that, compared to the slowness processing with the full array, the results obtained using only a 4-receiver subarray show a better correlation with GR and VCL, suggesting a stronger correlation between high-resolution processing results and physical properties of rocks. However, the correlation between slowness processing with a 2-receiver subarray and GR, VCL is lower, indicating that the small variations in the highest resolution processing result in this case. Figure 8b presents a crossplot of the slowness results from the full array processing of eight receivers

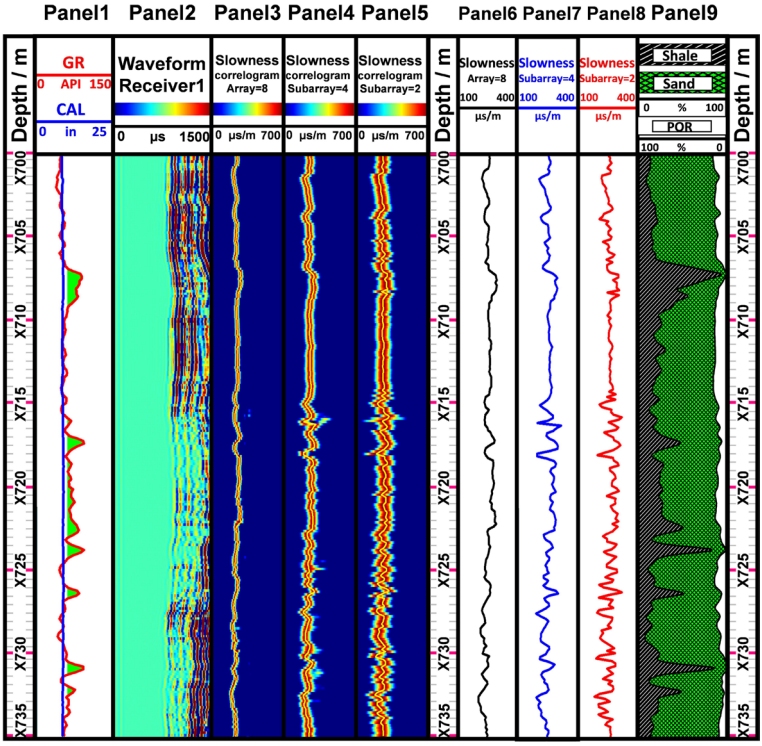

Fig. 7 Application of the proposed method to sandstone formation containing thin shale beds. Panel 1 shows the GR and borehole caliper log curve. Panel 2 shows the raw waveform of receiver 1 of the sonic array. The general trend of the semblance correlogram for 106.68 cm resolution (panel 3), 45.72 cm resolution (panel 4) and 15.24 cm resolution (panel 5) is consistent. The slowness curves corresponding to the three resolutions above are shown in panels 6–8. The results show that the slowness curves obtained with the proposed method are consistent with lithologic changes in sandstone formations containing thin-bedded shales

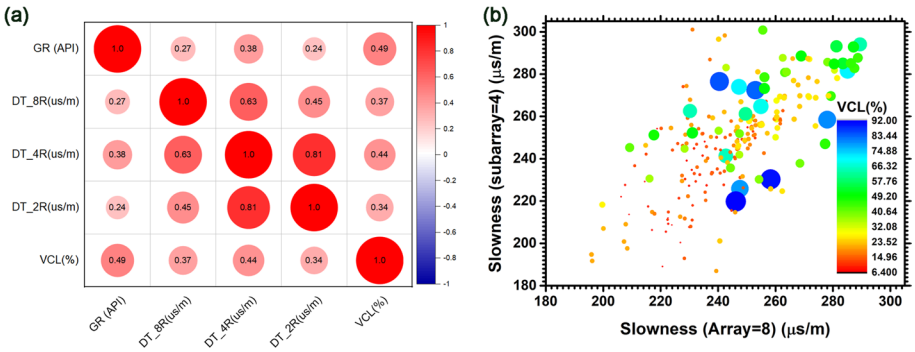

Fig. 8 **a** shows correlations among three slowness resolutions, GR, and VCL. Results from the 4-receiver subarray display a stronger link with GR and VCL compared to the full array, suggesting a closer tie between high-resolution processing and rock properties. **b** illustrates a crossplot of slowness results from eight receivers and 4-receiver subarray, with deviations mostly indicating higher VCL, highlighting the effectiveness of high-resolution slowness processing

and 4-receiver subarray processing, with different colors and sizes representing the levels of VCL. An intriguing observation is that the data points deviating from the diagonal mostly correspond to higher VCL, indicating that the high-resolution slowness processing corresponds to thin layers with higher VCL, demonstrating the effectiveness of high-resolution slowness processing.

It is worth noting that although high resolution provides a detailed characterization of the thin bed, other means are required to determine the true velocity of the thin bed due to measurement error and noise interference. Therefore, in practice it is generally recommended to process with different scales of resolution, and combined with gamma ray, porosity, or resistivity logs for the most realistic and effective determination of subarray aperture size. On the other hand, there is a limit to reducing the subarray aperture to improve resolution, which is related to the wavelength of the sonic wave in use. For waves with longer wavelengths, small aperture data processing will result in a distortion of the slowness curve.

5 Discussion

In this section, we will focus on the impact of subarray combinations on slowness estimation and analyze in detail the choice of resolution and the considerations that need to be taken into account.

The slowness resolution in sonic well logging is primarily determined by the processing aperture (resolution), as demonstrated by Hsu and Chang (1987), Valero et al. (2000), Zhang and Tang (2000), among others. While these studies achieved high-resolution slowness, the fidelity of slowness estimation was compromised due to low coherence signal-to-noise ratios. Traditional subarray methods have limitations in the available redundant information within the same depth interval. In addition, the number of waveforms that can be reconstructed varies for combinations of subarrays with different resolutions. At the highest resolution, for example (i.e., subarray aperture = 15.24 cm), the number of waveforms that can be reconstructed tends to be smaller due to the array span. As a result, slowness profiles may have a low S/N ratio. In response to this difficulty, this paper emphasizes how to leverage the SVI method to construct more waveform data usable for array coherence calculations from the limited redundant information (Al-Hagan et al. 2014). Meanwhile, this approach provides an alternative strategy for high-resolution processing in situations with poor signal quality and intense noise interference, overcoming the limitations of traditional subarray processing. The proposed method in this paper demonstrates robustness and high tolerance to data variations caused by noise. Numerical experiment results indicate its advantage in handling small-scale noise interference. Moreover, the available data quantity varies for different resolution combinations, allowing the adoption of different resolution processing strategies for varying levels of noise. Despite achieving high resolution for smaller processing apertures, the estimated slowness often lacks precision due to the lower signal-to-noise ratio in the calculated coherence maps. Additionally, for strong noise interference, combining filtering methods can enhance denoising effectiveness.

Furthermore, the advantage of this method lies in maximizing the extraction of useful formation signals in the measurement acquisition mode of borehole sonic logging. It is worth noting that, under normal conditions, the receiver spacing and depth movement distance are consistent, leading to signal overlap at the same depth processing interval. By recombining these signals, high-resolution processing can be achieved, simultaneously

improving the S/N ratio of the processing results. Additionally, in certain special cases, such as when the spacing between receivers and the depth movement distance are inconsistent or when receiver damage occurs within the receiving array, the method can still prove advantageous. Moreover, for specific lithologies like ultrafast formations (represented by tight sandstone, carbonate rocks, and basalt) and high-attenuation formations (represented by mudstone and shale, or shallow-sea formations), the useful formation signals collected by acoustic logging are typically very weak. In such cases, if interference signals such as noise are present, it can seriously disturb the assessment of the true nature of the formations. The method in this study is well-suited to address these challenging scenarios.

For field data, the choice of processing resolution should be carefully considered. Slowness logs in layered formations is affected by the sonic tool aperture. In the extraction of the properties, it is necessary to select an aperture smaller than the thickness of the thin layer. In reality, however, we do not know the true thickness of the formations in the underground. Other means are therefore required to determine the approximate boundaries of the thin layers. In addition, the use of multi-scale resolution to estimate slowness is firstly due to the fact that the actual thickness of the thin layer varies over a range within the measurement interval. A single vertical resolution treatment may ignore some stratigraphic response. Secondly, multi-scale processing, when combined with geological background and other geophysical logs, can help us filter out useless information. Subarray processing can provide quantitative slowness values in thin beds that are invisible to standard sonic tools, but the semblance of the stacked waveforms becomes susceptible to noise. And not only noise interference, instrument errors such as tool vibration (Song et al. 2017), cement bond, and tool eccentricity (Pardo et al. 2013) can affect the accuracy of the results. Thirdly, the use of subarrays with reduced spans to improve resolution has certain conditions of applicability. This treatment has a requirement for the wavelength of the sonic wave, i.e., its wavelength cannot be less than a quarter of the aperture of the subarray (Tang et al. 2004). Consequently, fast and slow layers within a borehole interval require different resolution strategies (Walker et al. 2019). However, compared to traditional conventional processing, this method may require more computational effort. Nevertheless, the increase in computational workload is not on a magnitude-changing scale, making it acceptable for practical data processing. Additionally, it is worth noting that for this method to effectively process signals, the prerequisite is that the collected signals must contain a certain amount of energy from the useful formation signals, even if the amplitude of these signals is relatively weak. This is a fundamental requirement for the effective application of all signal processing methods.

6 Conclusions

In this paper, we present a borehole slowness estimation method with enhanced resolution based on the reconstruction of neighboring virtual traces (RNVTs). The method combines subarray processing techniques with SVI-SNV, which exploits the nature of cross-correlation to generate a large amount of waveform data that can be used for slowness estimation, significantly improving the resolution and robustness of the estimated results.

The accuracy and reliability of proposed method was verified with synthetic examples. The results demonstrate that the proposed method can extract thin layer slowness with both high-resolution and S/N ratio. Furthermore, the results show that subarray aperture can be the main factors affecting the semblance results. Therefore, the processing resolution

should be chosen carefully. We then apply the method to field data and the estimated slowness is in good agreement with lithologic variations. Finally, we discuss the processing options for resolution, which may provide some guidance and reference for the application of the method to field data.

Acknowledgements This work was supported in part by was supported in part by the National Natural Science Foundation of China (42004097), in part by the Young-Talents-Project Start-up Foundation of Ocean University of China (202212017), and in part by the Young Elite Scientists Sponsorship Program by the China Association for Science and Technology (2019QNRC001). The authors would like to thank the Editor in Chief, Michael J. Rycroft, and three anonymous reviewers for their constructive comments and suggestions.

Data availability The authors are unable or have chosen not to specify which data have been used.

Declarations

Conflict of interest All authors declare that they have no conflict of interest.

References

Al-Hagan O, Hanafy SM, Schuster GT (2014) Iterative supervirtual refraction interferometry. Geophysics 79(3):Q21–Q30. https://doi.org/10.1190/geo2013-0210.1

Alshuhail A, Aldawood A, Hanafy S (2012) Application of super-virtual seismic refraction interferometry to enhance first arrivals: a case study from Saudi Arabia. The Leading Edge 31(1):34–39. https://doi.org/10.1190/1.3679326

An S, Hu T, Peng G (2017) Three-dimensional cumulant-based coherent integration method to enhance first-break seismic signals. IEEE Trans Geosci Remote Sens 55(4):2089–2096. https://doi.org/10.1109/TGRS.2016.2636336

Assous S, Elkington P, Linnett L (2014) Phase-based dispersion analysis for acoustic array borehole logging data. J Acoust Soc Am 135(4):1919–1928. https://doi.org/10.1121/1.4868396

Bader S, Wu X, Fomel S (2017) Semiautomatic seismic well ties and log data interpolation, pp 2381–2385. https://doi.org/10.1190/segam2017-17744197.1

Bassiouni Z (1994) Theory, measurement, and interpretation of well logs. Soc Pet Eng. https://doi.org/10.2118/9781555630560

Bharadwaj P, Schuster G, Mallinson I et al (2012) Theory of supervirtual refraction interferometry. Geophys J Int 188(1):263–273. https://doi.org/10.1111/j.1365-246X.2011.05253.x

Bharadwaj P, Wang X, Schuster G et al (2013) Increasing the number and signal-to-noise ratio of OBS traces with supervirtual refraction interferometry and free-surface multiples. Geophys J Int 192(3):1070–1084. https://doi.org/10.1093/gji/ggs087

Bharadwaj P, Schuster GT, Mallinson I (2011) Super-virtual refraction interferometry: Theory. In: SEG international exposition and annual meeting, SEG, pp SEG–2011. https://doi.org/10.1190/1.3628000

Bose S, Valero HP, Dumont A (2009) Semblance criterion modification to incorporate signal energy threshold. In: SEG technical program expanded abstracts 2009. Society of Exploration Geophysicists, pp 376–380

Brie A, Hsu K, Eckersley C (1988) Using the stoneley normalized differential energies for fractured reservoir evaluation. In: SPWLA Annual logging symposium, SPWLA, pp SPWLA–1988

Chen D, Guan W, Zhang C et al (2020) High-resolution inversion for dispersion characteristics of acoustic logging waveforms. J Geophys Eng 17(3):439–450. https://doi.org/10.1093/jge/gxaa003

Claerbout JF (1968) Synthesis of a layered medium from its acoustic transmission response. Geophysics 33(2):264–269. https://doi.org/10.1190/1.1439927

Coates R, Kane M, Chang C, et al (2000) Single-well sonic imaging: high-definition reservoir cross-sections from horizontal wells. In: SPE/CIM international conference on horizontal well technology, OnePetro. https://doi.org/10.2118/65457-MS

Dawood AA, Al-Shuhail A, Alshuhail A (2021) Enhancing the signal-to-noise ratio of sonic logging waveforms by super-virtual interferometric stacking. J Seism Explor 30(3):237–255

Dong S, Sheng J, Schuster GT (2006) Theory and practice of refraction interferometry, pp 3021–3025. https://doi.org/10.1190/1.2370154

Ekstrom MP (1995) Dispersion estimation from borehole acoustic arrays using a modified matrix pencil algorithm. In: Conference record of the twenty-ninth asilomar conference on signals, systems and computers, IEEE, pp 449–453. https://doi.org/10.1109/ACSSC.1995.540589
Franco JA, Ortiz MM, De GS et al (2006) Sonic investigation in and around the borehole. Oilfield Rev 18(1):14–31
Godio A, Dall'Ara A (2012) Sonic log for rock mass properties evaluation ahead of the tunnel face—a case study in the alpine region. J Appl Geophys 87:71–80. https://doi.org/10.1016/j.jappgeo.2012.09.007
Hanafy SM, AlHagan O, Al-Tawash F (2011) Super-virtual refraction interferometry: Field data example over a colluvial wedge. In: SEG international exposition and annual meeting, SEG, pp SEG–2011. https://doi.org/10.1190/1.3628001
Hanafy SM, Al-Hagan O (2012) Super-virtual refraction interferometry: an engineering field data example. Near Surface Geophys 10(5):443–449. https://doi.org/10.3997/1873-0604.2012032
Herrera RH, van der Baan M (2014) A semiautomatic method to tie well logs to seismic data. Geophysics 79(3):V47–V54. https://doi.org/10.1190/geo2013-0248.1
Hsu K, Baggeroer AB (1986) Application of the maximum-likelihood method (MLM) for sonic velocity logging. Geophysics 51(3):780–787. https://doi.org/10.1190/1.1442130
Hsu K, Chang S (1987) Multiple-shot processing of array sonic waveforms. Geophysics 52(10):1376–1390. https://doi.org/10.1190/1.1442250
Huang S, Torres-Verdín C (2016) Inversion-based interpretation of borehole sonic measurements using semianalytical spatial sensitivity functions. Geophysics 81(2):D111–D124. https://doi.org/10.1190/geo2015-0335.1
Huang S, Torres-Verdín C (2017) Fast-forward modeling of compressional arrival slowness logs in high-angle and horizontal wells. Geophysics 82(2):D107–D122. https://doi.org/10.1190/geo2016-0317.1
Huang S, Torres-Verdín C (2015) Sonic spatial sensitivity functions and inversion-based layer-by-layer interpretation of borehole sonic logs. In: SPWLA annual logging symposium, SPWLA, pp SPWLA–2015
Kazatchenko E, Markov M, Mousatov A (2003) Determination of primary and secondary porosity in carbonate formations using acoustic data. In: SPE Annual technical conference and exhibition? SPE, pp SPE–84,209. https://doi.org/10.2118/84209-MS
Khadhraoui B, Kisra S, Nguyen H (2018) A new algorithm for high depth resolution slowness estimate on sonic-array waveforms. In: SPWLA Annual Logging Symposium, SPWLA, p D053S012R001
Kimball CV, Marzetta TL (1984) Semblance processing of borehole acoustic array data. Geophysics 49(3):274–281
Kosloff DD, Baysal E (1982) Forward modeling by a Fourier method. Geophysics 47(10):1402–1412. https://doi.org/10.1190/1.1441288
Kosloff D, Reshef M, Loewenthal D (1984) Elastic wave calculations by the Fourier method. Bull Seismol Soc Am 74(3):875–891. https://doi.org/10.1785/BSSA0740030875
Kozak M, Williams J (2015) Instantaneous frequency-slowness analysis applied to borehole acoustic data. ASEG Ext Abstr 2015(1):1–5. https://doi.org/10.1071/ASEG2015ab159
Kozak M, Kozak M, Williams J (2006) Identification of mixed acoustic modes in the dipole full waveform data using instantaneous frequency-slowness method. In: SPWLA Annual Logging Symposium, SPWLA, pp SPWLA–2006
Lang S, Kurkjian A, McClellan J et al (1987) Estimating slowness dispersion from arrays of sonic logging waveforms. Geophysics 52(4):530–544. https://doi.org/10.1190/1.1442322
Lei T, Zeroug S, Bose S et al (2019) Inversion of high-resolution high-quality sonic compressional and shear logs for unconventional reservoirs. Petrophysics 60(06):697–711. https://doi.org/10.30632/PJV60N6-2019a1
Li W, Tao G, Matuszyk PJ et al (2015) Forward and backward amplitude and phase estimation method for dispersion analysis of borehole sonic measurements. Geophysics 80(3):D295–D308. https://doi.org/10.1190/geo2014-0298.1
Liang S, Hu T, Cui D et al (2020) Weak signal enhancement using adaptive local similarity and neighboring super-virtual trace for first arrival picking. J Geophys Eng 17(6):1005–1015. https://doi.org/10.1093/jge/gxaa059
Lu K, Liu Z, Hanafy S et al (2020) Noise reduction with reflection supervirtual interferometry. Geophysics 85(3):V249–V256. https://doi.org/10.1190/tle39070518.1
Ma R, Zou Z, Rui Y et al (2018) A composite absorbing boundary based on the SPML and sponge absorbing boundary for pseudo-spectral elastic wave modeling. Geophys Prospect Pet 57(1):94–103
Maalouf E, Torres-Verdín C (2018) Interpretation of borehole sonic measurements acquired in vertical transversely isotropic formations penetrated by vertical wells. Geophysics 83(6):D187–D202. https://doi.org/10.1190/geo2017-0757.1

Maalouf E, Torres-Verdín C (2018) Inversion-based method to mitigate noise in borehole sonic logs. Geophysics 83(2):D61–D71. https://doi.org/10.1190/geo2017-0334.1
Mahiout S, Torlov V, Gouda M, et al (2022) High resolution acoustic analysis for improved formation evaluation of carbonate and clastic reservoirs. OnePetro, p D021S064R003. https://doi.org/10.2118/211603-MS
Mallinson I, Bharadwaj P, Schuster G et al (2011) Enhanced refractor imaging by supervirtual interferometry. The Leading Edge 30(5):546–550. https://doi.org/10.1190/1.3589113
Ma J, Matuszyk PJ, Mallan RK, et al (2010) Joint processing of forward and backward extended prony and weighted spectral semblance methods for robust extraction of velocity dispersion data. In: SPWLA Annual Logging Symposium, SPWLA, pp SPWLA–2010
McFadden P, Drummond B, Kravis S (1986) The nth-root stack: theory, applications, and examples. Geophysics 51(10):1879–1892. https://doi.org/10.1190/1.1442045
Montmayeur H, Graves R (1985) Prediction of static elastic/mechanical properties of consolidated and unconsolidated sands from acoustic measurements: basic measurements. In: SPE Annual Technical Conference and Exhibition? SPE, pp SPE–14,159. https://doi.org/10.2118/14159-MS
Mukhopadhyay P, Cheng A, Tracadas P (2013) The differential-phase based time-and frequency-semblance algorithm for array-acoustic processing and its application to formation-slowness measurement. Petrophysics 54(05):475–481
Neidell NS, Taner MT (1971) Semblance and other coherency measures for multichannel data. Geophysics 36(3):482–497
Nolte B, Rao R, Huang X (1997) Dispersion analysis of split flexural waves. Tech. rep., Massachusetts Institute of Technology. Earth Resources Laboratory
Oyler DC, Mark C, Molinda GM (2008) Correlation of sonic travel time to the uniaxial compressive strength of us coal measure rocks. In: Proceedings of the 27th international ground control in mining conference, Morgantown, WV, pp 338–346
Paillet FL, Cheng CH (1991) Acoustic waves in boreholes. CRC Press, Boca Raton
Pardo D, Matuszyk PJ, Torres-Verdin C et al (2013) Influence of borehole-eccentred tools on wireline and logging-while-drilling sonic logging measurements. Geophys Prospect 61(s1):268–283. https://doi.org/10.1111/1365-2478.12022
Peyret A, Torres-Verdin C, Xu Y (2006) Assessment of shoulder-bed, invasion, and lamination effects on borehole sonic logs: a numerical sensitivity study. In: SPWLA Annual Logging Symposium, SPWLA, pp SPWLA–2006
Qiao BP, Guo P, Wang P et al (2014) Effectively picking weak seismic signal near the surface based on reverse virtual refraction interferometry. Chin J Geophys 57(6):1900–1909. https://doi.org/10.6038/cjg20140621
Qiao B, Guo P, Wang P et al (2015) Retrieval of super-virtual refraction by cross-correlation. Geophys Prospect 63(3):552–566. https://doi.org/10.1111/1365-2478.12202
Razak MA, Ashqar A, Das S, et al (2021) Advances in cased hole acoustic slowness measurements and its application in a depleted reservoir drilled with highly inclined well: a case study from offshore Malaysia. In: International petroleum technology conference, IPTC, p D031S008R002. https://doi.org/10.2523/IPTC-21154-MS
Schuster GT (2009) Seismic interferometry. Cambridge University Press, Cambridge
Song X, Zhao Y, Dykstra J (2017) Active damping of acoustic ringing effect for oil well sonic logging system. IEEE Trans Ind Electron 64(4):3423–3432. https://doi.org/10.1109/TIE.2016.2598315
Song L, Zou Z, Huang Z (2019) Supervirtual refraction interferometry based on stacking of neighboring virtual-traces and its application to enhancing wide-angle OBS refraction waves. Chin J Geophys 62(3):993–1006
Sun X, Ayadiuno C, Li W (2019a) A statistical prony method for shear slowness estimation from dipole measurements. In: SEG International exposition and annual meeting, SEG, p D043S129R005
Sun X, Ayadiuno C, Li W (2019b) A statistical Prony method for shear slowness estimation from dipole measurements, pp 859–863. https://doi.org/10.1190/segam2019-3216002.1
Tang XM (1997) Predictive processing of array acoustic waveform data. Geophysics 62(6):1710–1714. https://doi.org/10.1190/1.1444270
Tang X, Reiter E, Burns D (1995) A dispersive-wave processing technique for estimating formation shear velocity from dipole and Stoneley waveforms. Geophysics 60(1):19–28. https://doi.org/10.1190/1.1443747
Tang XM, Cheng CHA, Cheng A (2004) Quantitative borehole acoustic methods, vol 24. Elsevier, Amsterdam

Tang X, Patterson D (2001) Detecting thin gas beds in formations using Stoneley wave reflection and high-resolution slowness measurements. In: SPWLA Annual Logging Symposium, SPWLA, pp SPWLA–2001

Valero HP, Hsu K, Brie A (2000) Multiple-shot processing in slowness and time domain of array sonic waveforms. In: SEG international exposition and annual meeting, SEG, pp SEG–2000. https://doi.org/10.1190/1.1815743

Walker K, Sun Q, Wang R (2019) Wavelength-based axial resolution limitations of flexural wave dispersion sonic logging. In: SPWLA Annual Logging Symposium, SPWLA, p D043S012R002

Walls J (1987) Poisson's ratio and mechanical properties from core and well log measurements. Paper SPE 16795, pp 27–30

Wang R, Qiao W, Ju X (2012) A multi-channel acoustic logging signal dispersion analysis method. Well Logging Technol. 36(2):135–140. https://doi.org/10.16489/j.issn.1004-1338.2012.02.006

Wang R, Coates R, Zhao J (2021) Borehole sonic data dispersion analysis with a modified differential-phase semblance method. Petrophysics 62(04):379–392. https://doi.org/10.30632/PJV62N4-2021a3

Wang R, Hornby B, Walker K et al (2021) Advanced monopole and dipole sonic log data processing—part 1: real time. Geophysics 86(2):D77–D91. https://doi.org/10.1190/geo2020-0326.1

Wang R, Hornby B, Chang C, et al (2018) Enhanced-resolution dipole sonic logging data processing. In: SEG technical program expanded abstracts 2018. Society of exploration geophysicists, pp 679–683. https://doi.org/10.1190/segam2018-2995738.1

Wapenaar K, Fokkema J (2006) Green's function representations for seismic interferometry. Geophysics 71(4):SI33–SI46. https://doi.org/10.1190/1.2213955

Wapenaar K, Draganov D, Snieder R et al (2010) Tutorial on seismic interferometry: part 1—basic principles and applications. Geophysics 75(5):75A195-75A209. https://doi.org/10.1190/1.3457445

Wapenaar K, Slob E, Snieder R et al (2010) Tutorial on seismic interferometry: part 2—underlying theory and new advances. Geophysics 75(5):75A211-75A227. https://doi.org/10.1190/1.3463440

Wapenaar K, Draganov D, van der Neut J, et al (2005) Seismic interferometry: a comparison of approaches, pp 1981–1984. https://doi.org/10.1190/1.1851182

Xu S (2023) Acoustic-wave radiations of mono- and dual-sources in poorly bonded cased boreholes: modeling and field applications. IEEE Trans Geosci Remote Sens 61:1–10. https://doi.org/10.1109/TGRS.2023.3249250

Xu S (2023) Integrated multipole acoustic modeling and processing in general stressed formations, part 1: an effective approach study. Geoenergy Sci Eng 228(211):981. https://doi.org/10.1016/j.geoen.2023.211981

Xu S, Zou Z (2023) Supervirtual interferometry as a tool for slowness estimation of logging-while-drilling multipole acoustic data. IEEE Trans Geosci Remote Sens 61:1–16. https://doi.org/10.1109/TGRS.2023.3274517

Xu S, Su YD, Tang XM (2017) A super-mixing-virtual interferometric array signal processing technique and its applications to cased-hole acoustic logging. Chin J Geophys 60(7):2904–2912. https://doi.org/10.6038/cjg20170734

Xu S, Zou Z, Tang X (2022) Estimation of elastic wave velocity from logging-while-drilling measurement in unconsolidated formation of accretionary wedge in nankai trough. IEEE Trans Geosci Remote Sens 60:1–13. https://doi.org/10.1109/TGRS.2022.3219083

Xu X, Zou Z, Han M et al (2023) Deep-learning velocity model building by jointly using seismic first arrivals and early-arrival waveforms. Chin J Geophys. https://doi.org/10.6038/cjg2023Q0847. (**in Chinese**)

Zeng F, Yue W, Li C (2018) Dispersion analysis of borehole sonic measurements by Hilbert transform and band-pass filters. Geophysics 83(4):D127–D150. https://doi.org/10.1190/geo2017-0580.1

Zeroug S, Sinha BK, Lei T et al (2018) Rock heterogeneity at the centimeter scale, proxies for interfacial weakness, and rock strength-stress interplay from downhole ultrasonic measurements. Geophysics 83(3):D83–D95. https://doi.org/10.1190/geo2017-0049.1

Zhang T, Tang X (2000) Waveform inversion of array acoustic log data for high-resolution formation slowness estimation. In: SEG technical program expanded abstracts 2000. Society of exploration geophysicists, pp 1683–1686. https://doi.org/10.1190/1.1815742

Authors and Affiliations

Song Xu[1,2,3] · Shun Li[1] · Zhihui Zou[1,2,3]

✉ Song Xu
xusongupc@sina.com

Shun Li
lishun4199@stu.ouc.edu.cn

Zhihui Zou
zouzhihui@ouc.edu.cn

[1] Key Laboratory of Submarine Geosciences and Prospecting Techniques, Ministry of Education (MOE), College of Marine Geosciences, Ocean University of China, Qingdao 266100, Shandong, China

[2] Evaluation and Detection Technology Laboratory of Marine Mineral Resources, Qingdao National Laboratory for Marine Science and Technology, Qingdao 266061, Shandong, China

[3] Frontiers Science Center for Deep Ocean Multispheres and Earth System, Ocean University of China, Qingdao 266100, Shandong, China